Research Article | Vol. 2, No. 10 / 15 Oct 2023 / Optics Continuum 2215

OPTICS CONTINUUM

Investigation of modified uni-traveling carrier photodiode for cryogenic microwave photonic links

CARSON MOSELEY,[1,†] SUMMER BOLTON,[1,†] JOSEPH M. LUKENS,[2,3,8] YUN-YI PAI,[4,5] MICHAEL CHILCOTE,[4,6] BENJAMIN J. LAWRIE,[4] SHUNQIAO SUN,[1] MADDY WOODSON,[7] STEVEN B. ESTRELLA,[7] SEONGSIN M. KIM,[1] AND PATRICK KUNG[1,9]

[1]*Electrical and Computer Engineering, The University of Alabama, Tuscaloosa, Alabama 35487, USA*
[2]*Research Technology Office and Quantum Collaborative, Arizona State University, Tempe, Arizona 85287, USA*
[3]*Quantum Information Science Section, Oak Ridge National Laboratory, Oak Ridge, Tennessee 37831, USA*
[4]*Materials Science and Technology Division, Oak Ridge National Laboratory, Oak Ridge, Tennessee 37831, USA*
[5]*Apple, Cupertino, California 95014, USA*
[6]*Sandia National Laboratories, Albuquerque, New Mexico 87123, USA*
[7]*Freedom Photonics, Santa Barbara, California 93117, USA*
[8]*joseph.lukens@asu.edu*
[9]*patkung@eng.ua.edu*
[†]These authors contributed equally to this paper.

Abstract: Quantum devices present the potential for unparalleled computing and communications capabilities; however, the cryogenic temperatures required to successfully control and read out many qubit platforms can prove to be very challenging to scale. Recently, there has emerged an interest in using microwave photonics to deliver control signals down to ultracold stages via optical fiber, thereby reducing thermal load and facilitating dense wavelength multiplexing. Photodetectors can then convert this optical energy to electrical signals for qubit control. The fidelity of the quantum operations of interest therefore depend heavily upon the characteristics of the photodiode, yet experimental demonstrations of fiber-coupled photodetection systems at low temperatures are relatively few in number, leaving important open questions regarding how specific detectors may perform in real-world cryogenic settings. In this work, we examine a highly linear modified uni-traveling carrier photodiode (MUTC-PD) under C-band illumination (1530–1565 nm) at three temperature regimes (300 K, 80 K, and ~4 K) and multiple bias conditions. Our findings of reduced responsivity but preserved bandwidth are consistent with previous studies, while our saturation tests suggest a variety of potential applications for MUTC-PDs in cryogenic microwave photonics with and without electrical bias. Overall, our results should provide a valuable foundation for the continued and expanding use of this detector technology in quantum information processing.

1. Introduction

Given the variety of technologies currently being explored for quantum computing, it is expected that quantum networks—infrastructures that transmit quantum information and establish entanglement between distributed quantum resources—will need to support an array of heterogenous systems [1]. Many of these platforms, such as superconducting circuits [2] and silicon qubits [3], rely on precise microwave control pulses and sequences for the realization of high-fidelity

#502533 https://doi.org/10.1364/OPTCON.502533
Journal © 2023 Received 7 Aug 2023; accepted 28 Sep 2023; published 11 Oct 2023

OPTICS CONTINUUM

quantum gates. Yet their required operating temperatures (<1 K) present two major challenges for scaling to many qubits: first, blackbody radiation introduces a significant thermal load in the microwave domain, thereby demanding heavy radio-frequency (RF) attenuation between stages in a dilution refrigerator; second, as the number of qubits grows, so does the number of required coaxial cables, which are in turn ultimately limited by the dilution refrigerator dimensions and cooling power [4].

Microwave photonics [5,6] offers the potential to address both limitations, by using microwave control signals to modulate optical fields at room temperature, delivering these photonic waveforms to a cryogenic environment via optical fiber, and then converting the optical waveforms back to microwave signals on a fast photodiode. The reduced thermal load at optical wavelengths, coupled with parallelization through wavelength-division multiplexing, can in principle enable the use of orders of magnitude more qubits in a single dilution refrigerator than is possible with coaxial cable. A seminal recent experiment has highlighted the feasibility of this approach in the context of a superconducting transmon qubit [7], while other work has explored cryogenic photodetection for biasing of superconducting nanowire single-photon detectors—a task distinct from direct qubit control but enjoying similar potential thermal advantages [8]. Additionally, microwave photonic links at 4 K can be leveraged for driving superconducting Josephson junction arrays, an application where relatively high (milliamp-scale) photocurrents can prove useful [9,10].

Link performance for quantum control with microwave photonics will depend heavily on the photodiode's ability to realize optical-to-electrical (OE) conversion with high efficiency, wide bandwidth, and high linearity at cryogenic temperatures. Previous investigations into cryogenic OE conversion for p-i-n [11], uni-traveling carrier [12–15], and modified uni-traveling carrier [16–18] photodiodes have generally confirmed the preservation of high RF bandwidth down to few-kelvin temperatures, with reduced responsivity in the C-band (1530–1565 nm) due to bandgap widening in InGaAs. Linearity is likewise a critical feature of photodetectors in analog photonics; a highly linear photodiode is able to implement OE conversion in which the output photocurrent is a scaled replica of the input optical power with minimal distortion [19]. To our knowledge, only two experiments have performed photodiode linearity tests at cryogenic temperatures: one that focused on amplitude-to-phase modulation conversion [16], and another that concentrated on microwave powers below −50 dBm [17]. Accordingly, the extent to which these devices can support significantly higher powers represents an important unmet gap in the continued development of ultracold microwave photonic links.

In this work, we test a modified uni-traveling carrier photodiode (MUTC-PD) designed for high saturation currents at 300 K, 80 K, and ∼4 K. After confirming low dark current and a responsivity that drops as expected with temperature, we probe RF bandwidth with an optical heterodyne setup comprising two lasers with detuned frequencies. Bandwidth does not vary with temperature, but it does vary significantly with bias voltage in agreement with expectations. Finally, we use an erbium-doped fiber amplifier (EDFA) to increase incident optical power up to ∼100 mW, measuring the RF output at test frequencies of 3 GHz and 10 GHz. Up to our maximum available optical power, no appreciable compression is observed under −5 V bias; for 0 V bias, however, the output saturates beyond approximately 10 mA of DC photocurrent. For the examined device, the saturation power appears to increase with reducing temperatures. Because the high saturation currents observed with this detector enable work with optical powers of order 100 mW, intriguing opportunities tied to highly multiplexed signal delivery and high-power RF pumping emerge. Admittedly, the photodiode cannot reasonably be installed on the mixing chamber of a dilution refrigerator for such use cases because of insufficient cooling power. However, fiber delivery of multiplexed RF signals to a detector held at 4 K followed by superconducting coaxial delivery from 4 K to the mixing chamber still addresses many problems associated with semirigid coaxial

OPTICS CONTINUUM

cables and enables fundamentally new research directions in the control of superconducting quantum devices, thereby contributing to emerging applications in quantum networking.

2. Background

2.1. Photodiode design

An MUTC-PD [19–22] is a unique photodiode architecture that enables the design of devices that saturate at high levels of input optical power, building off the uni-traveling carrier photodiode (UTC-PD) [23]. As such, MUTC-PDs can support high frequencies as well, with recent demonstrations exceeding 200 GHz [24]. A traditional UTC-PD employs a *p*-doped absorber which generates electron-hole pairs. The photogenerated electrons move into a wider-bandgap collector layer, which is depleted with appropriate reverse bias, and the electrons accelerate through this layer to be collected at the *n*-contact. A wide-bandgap barrier layer blocks electron diffusion to the *p*-contact. Meanwhile, the photogenerated holes are collected immediately (hence the term "uni-traveling" carrier). An MUTC-PD leverages the UTC-PD structure, with some improvements to further combat electric field collapse through the space-charge effect, as well as a modification to the absorber such that it is partially depleted (i.e., consisting of both a *p*-doped layer and depleted layer). Figure 1 shows a representative band diagram (a) and device structure (b) for an MUTC-PD of the form used in the tests here. Our specific MUTC-PD is fabricated by Freedom Photonics [25,26] and designed for high-photocurrent operation, optimized for a direct current (DC) bias of −5 V. Due to the electric field induced by the generated carriers, the RF bandwidth can actually increase with power in these devices [20]; for the particular MUTC-PD under test, the nominal 3 dB bandwidth is approximately 10 GHz (15 GHz) at 10 mA (20 mA) DC photocurrent at room temperature.

2.2. Experimental methods

Figure 2 illustrates the experimental setup used to characterize the device. The heterodyne beat method [6] is used to generate an RF signal by mixing two slightly detuned continuous-wave (CW) lasers, which are coupled into fiber before being fed through a polarization controller, designed to align polarization for maximum modulation efficiency. The optical signals are combined in a single-mode fiber coupler, and then fed through a single-mode polarizer. CW Laser 1 (QPhotonics) is configured at a fixed wavelength of 1536.43 nm (195.123 THz). The emission frequency of CW Laser 2 (Pure Photonics) is tunable between 191.5–196.5 THz in 100 MHz steps, corresponding to a wavelength range of 1565–1525 nm. The fast MUTC-PD is optically connected to the output of the polarizer, and converts the mixed laser beams into a microwave signal at their difference frequency.

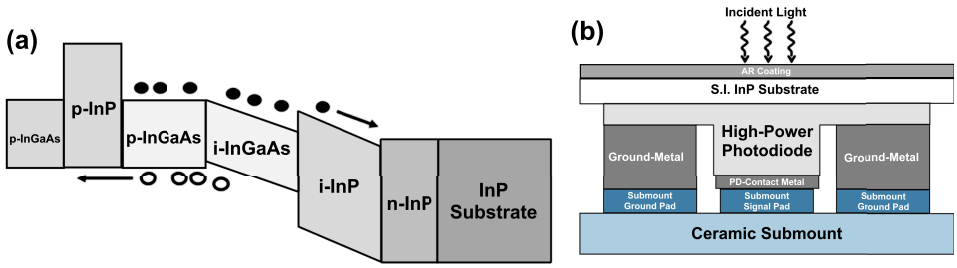

Fig. 1. (a) Simplified illustrated band diagram of an MUTC-PD structure and (b) cross-section of a backside-illuminated, high-power MUTC-PD bonded to a ceramic submount.

For ≥80 K measurements, the fiber-pigtailed MUTC-PD is mounted in a liquid nitrogen cryostat (Cryo Industries of America), and for ~4 K measurements, it is mounted in a dilution

OPTICS CONTINUUM

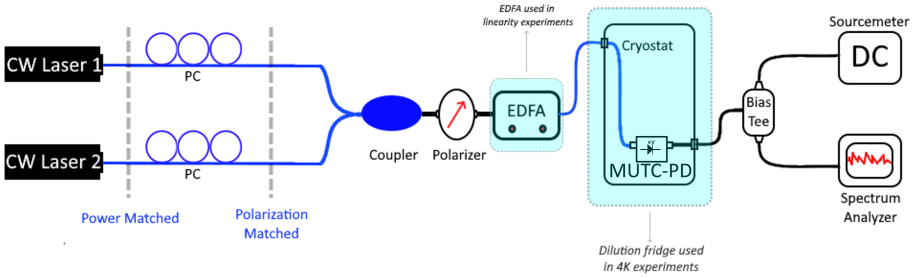

Fig. 2. Experimental setup for MUTC-PD characterization. The optical path includes two CW laser sources, one fixed at 1536.43 nm and the other tunable in the range 1525–1565 nm, with matched output powers and polarizations (PC: polarization controller); an optical coupler; a polarizer; an EDFA (for saturation measurements only); a fiber feedthrough; and a cold stage (cryostat or dilution refrigerator) in which the MUTC-PD is located. The electrical path includes an RF cable attached to the MUTC-PD and a feedthrough, an external bias tee, a sourcemeter unit that provides DC biasing, and a spectrum analyzer for RF output power measurements.

refrigerator (Leiden Cryogenics) on a cold-insertable probe. Under normal circulation, the system has approximately 200 μW of cooling power (rated at 100 mK) at the mixing chamber stage of the probe, where the detector is thermally anchored; ambient temperature is measured by a thermometer approximately 1–2 mm away from the MUTC-PD. A fiber patch cord carries the combined laser signals from the output of the polarizer to the input of a hermetic fiber feedthrough on the vacuum chamber. The detector is connected to an external bias tee via semirigid coax. A sourcemeter provides DC bias to the detector and measures the DC photocurrent, while the pure RF signal is measured by an electrical spectrum analyzer. In addition to measurements at −5 V bias (the detector design point), we perform tests at 0 V bias as well. Zero-bias operation appears particularly interesting for cryogenic microwave photonics, for it eliminates the need for a power supply, alleviates electrical crosstalk in photodiode arrays, and permits a smaller footprint without bulky bias circuity [27]. Reduced power dissipation is also possible [17], as evident from the bias-dependent term in the standard power conversion efficiency formula [6]. Moreover, even for photodiodes anchored to the 4 K plate of a dilution refrigerator, watts of laser power would introduce problematic levels of heating. Thus, zero-bias operation enables meaningful saturation measurements using laser powers of up to 100 mW without introducing unmanageable levels of heating at 4 K.

The dark current-voltage characteristics of the MUTC-PD were measured for biases of −5.0 V to +0.5 V at all temperatures tested. To ensure the integrity of the devices after repeated optical excitation and thermal cycling, dark current measurements were conducted both before and after each test described below. In all instances, the measured dark current remained consistently below 10 nA (the resolution limit of our sourcemeter), confirming the reliability and stability of the device.

3. Results and discussion

3.1. Wavelength-dependent responsivity

We first characterized the DC responsivity at a reverse bias of −5 V using CW Laser 2 as the sole excitation source, scanning the wavelength range 1525–1565 nm at a nominal laser output of 15.8 mW. The optical power reaching the MUTC-PD was measured with a calibrated power meter, while the DC current was recorded using the sourcemeter: the ratio defines the responsivity $\mathcal{R}$ in units of A/W. The photocurrent consists of the difference between the measured current and

OPTICS CONTINUUM

the dark current at −5 V. Figure 3 compares the responsivity spectra at three test temperatures, where the 1.5 K test was performed on the dilution refrigerator mixing chamber, resulting in steady-state operation at 1.5 K due to the substantial heat load provided by the laser excitation (operating here on the mixing chamber allowed us to identify the limits of operation at the minimum accessible temperature for these laser powers). The responsivity decreases when the temperature is lowered. Additionally, at 300 K, the responsivity remains relatively stable at 0.3–0.4 A/W across the measured wavelengths. At 80 K, it exhibits a slight monotonic decrease from ~0.2 A/W to ~0.1 A/W with increasing wavelength. The decline in responsivity with wavelength is more pronounced at 1.5 K, where it decreases from 0.06 A/W to 0.01 A/W. These observations can be attributed to the widening of the bandgap in the MUTC-PD photoabsorbing material at lower temperature, which blueshifts the peak absorption wavelength and significantly reduces efficiency in the C-band, consistent with previous observations [12]. We confirm this explanation for the responsivity reduction by measuring the photocurrent at 1.5 K for a CW laser at 1062 nm (comfortably away from the bandgap), obtaining 0.22 A/W, equivalent to 0.32 A/W at 1550 nm for a fixed quantum efficiency—more than an order of magnitude larger than the measured 1550 nm responsivity at 1.5 K. These findings reaffirm that the observed responsivity reduction is primarily caused by the widening of the material bandgap and not thermally induced optical misalignment, which would have been expected to impact both 1062 nm and 1550 nm in comparable fashions.

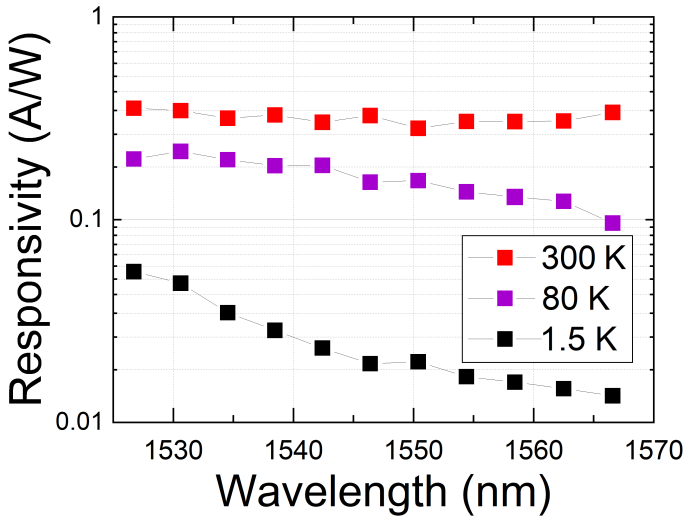

Fig. 3. Spectrally dependent responsivity of MUTC-PD at different temperatures under −5 V bias.

3.2. RF bandwidth

With both lasers on and CW Laser 2 systematically detuned from CW Laser 1 at 1536.43 nm , we obtained the frequency response curves shown in Fig. 4. The total optical power reaching the MUTC-PD was 10.9 mW for these tests, corresponding to DC photocurrents of 4.3 mA at 300 K and 2.2 mA at 80 K. (Due to the lower responsivity, we were unable to obtain a sufficient signal-to-noise ratio to determine the RF bandwidth at 1.5 K with the same optical power, so we include 300 K and 80 K results only.) Figures 4(a) and 4(b) plot the measured RF output power as a function of frequency for bias conditions of −5 V and 0 V, respectively, obtained after backing out the measurement system's frequency response (bias tee and cables) characterized with a

OPTICS CONTINUUM

vector network analyzer. With fixed optical power and, therefore, different DC photocurrent, the 3 dB bandwidth at −5 V bias extends to approximately 15 GHz at 300 K, compared to 12 GHz at 80 K. At 0 V bias, the respective 3 dB bandwidths reduce significantly, to about 7 GHz at 300 K and 5 GHz at 80 K.

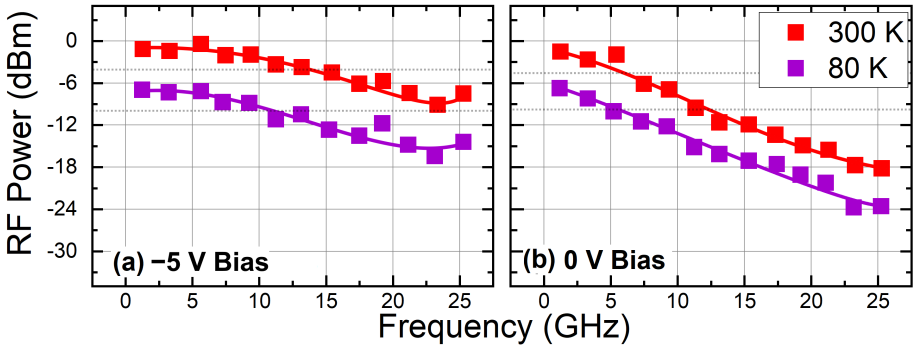

Fig. 4. RF output of MUTC-PD as a function of frequency at (a) −5 V bias and (b) 0 V bias. The DC photocurrent is 4.3 mA at 300 K and 2.2 mA at 80 K.

The relatively close RF bandwidths at 300 K and 80 K for a given bias point are consistent with previous cryogenic photodetection studies in p-i-n photodiodes [11], where the slight reduction observed at 80 K in our case is likely due to the lower DC photocurrent [21,22,25], rather than other thermal effects. On the other hand, the striking difference in bandwidth as a function of bias can be attributed to the space-charge screening effect, discussed further in the saturation tests below.

3.3. Saturation

The linearity of a photodetector response as a function of optical excitation power is important for ensuring reliable OE conversion and maximizing output powers in microwave photonics [19]. At first glance, linearity may not appear particularly important for cryogenic quantum control applications, due to the low powers involved. For example, in the recent demonstration of microwave-photonic control of a transmon qubit [7], photocurrents $\lesssim$ 20 μA were employed—orders of magnitude below the tens of milliamps typical for reaching compression with MUTC-PDs at room temperature [21,22]. Nevertheless, highly linear photodetection can still prove important for distortion-free electrical multiplexing of multiple control signals on a single detector [17], and microwave powers in the watt range are not uncommon for manipulating spins in optically detected magnetic resonance—e.g., with nitrogen-vacancy centers in diamond [28] or hexagonal boron nitride [29]. Admittedly, the thermal load produced at such high powers can easily surpass the cooling capacities of commercial dilution refrigerators at a given temperature, an effect clearly observed in our tests here. On the other hand, cooling limitations can be alleviated dramatically under low-duty-cycle excitation with the same peak power [7]. Ultimately, the suitability of microwave photonics for any cryogenic system is application-dependent and so beyond the scope of the current investigation; here, we focus on the raw OE performance in order to inform any such future implementations.

The experimental setup remained the same as in Fig. 2, with the EDFA in place at the output of the polarizer before the optical fiber feedthrough. The powers of both lasers were again manually matched prior to entering the EDFA. The RF power and frequency were measured on the spectrum analyzer as the EDFA pump current was gradually increased. For each configuration, optical powers in the range 8–100 mW entered the feedthrough, as confirmed independently with a calibrated power meter. We considered biases of −5 V and 0 V and temperatures of 300 K,

OPTICS CONTINUUM

80 K, and 6.6 K. For 100 mW continuous laser illumination, operation on the mixing chamber during mixture circulation is infeasible, so these measurements were performed with the detector mounted to the 4 K plate, and the actual temperature at the MUTC-PD during the measurement varied between 5.25 K and 7.80 K with a median of 6.6 K, which we use here to label the relevant test results. We considered two RF frequencies: 3 GHz, comparable to resonant transitions in typical solid-state spin systems [28,29]; and 10 GHz, comfortably within the 3 dB bandwidth at −5 V bias but not at 0 V (cf. Fig. 4), in order to emphasize bandwidth effects at the two operating points.

To assess the saturation characteristics, the measured RF output power is plotted against the detected optical excitation power as represented by the DC photocurrent. The collected data are summarized in Fig. 5. For comparison, the measured powers are plotted against the ideal case of 100% percent optical modulation, i.e., for a sinusoidal signal with peak photocurrent equal to the DC average: $P_{\text{ideal}} = \frac{1}{2} Z I_D^2$, where $Z = 50\ \Omega$ and I_D is the DC photocurrent. Attainment of this ideal value assumes perfect power balancing of the two heterodyne lasers, along with instantaneous and linear OE conversion.

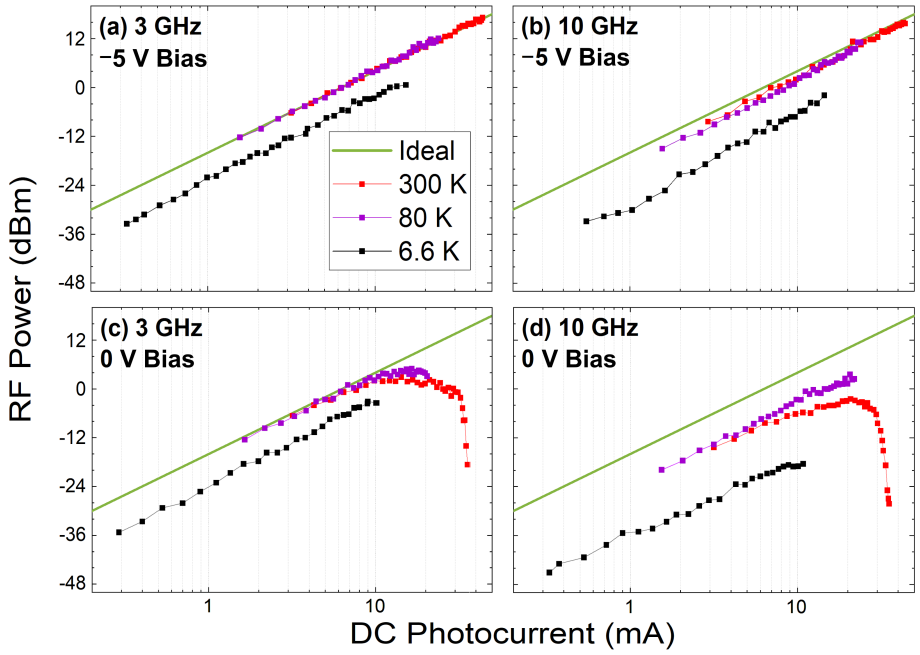

Fig. 5. RF output power from MUTC-PD as a function of DC photocurrent, measured using the optical heterodyning method where the mixed lasers are amplified through an EDFA prior to being sent to the device. The straight green line corresponds to the ideal case of 100% modulation contrast. (a) 3 GHz, −5 V bias. (b) 10 GHz, −5 V bias. (c) 3 GHz, 0 V bias. (d) 10 GHz, 0 V bias.

In Fig. 5(a), the output characteristics under −5 V bias and at 3 GHz are compared at different temperatures. The measured data for both the 300 K and 80 K conditions closely match the ideal line, with the 80 K results spanning lower photocurrents due to the reduced responsivity at this temperature (Fig. 3). In addition to further shifts to the left for the 6.6 K data due to this responsivity effect, the RF output power drops to about 6 dB below the ideal line as well, which we surmise can be attributed to a higher RF loss through the cables used in the dilution refrigerator. Despite this, the data points remain parallel to the ideal line. As such, no saturation or output roll-off was observed for the range of optical excitations used at −5 V bias and 3 GHz.

OPTICS CONTINUUM

Figure 5(b) summarizes data of a similar study at 10 GHz, with the bias maintained at −5 V. No appreciable output compression is observed under these conditions either. The measured data at 300 K and 80 K remain closely matched to the ideal line, even improving in agreement as power increases. These results are consistent with the RF response of the device shown in Fig. 4(a)—accounting for the DC photocurrents there (4.2 mA at 300 K and 2.2 mA at 80 K)—as well as the bandwidth improvements with increased photocurrent common in MUTC-PDs [21,22,25].

Now, under zero-bias conditions, more intriguing behavior for MUTC-PD saturation appears, as a function of both temperature and RF frequency. Figure 5(c) summarizes the device saturation characteristics at the three temperatures and 3 GHz. In contrast to the −5 V bias case [Fig. 5(a)], the RF output powers at both 300 K and 80 K clearly reach a saturation point for photocurrents above roughly 10 mA, while adhering to the ideal line for lower photocurrents. The zero-bias results at 10 GHz follow in Fig. 5(d). Due to the lower RF bandwidth at 0 V compared to −5 V [as demonstrated in Fig. 4(b)], the measured RF output power is noticeably lower than at −5 V bias at all temperatures. Output saturation remains quite evident, with an onset close to 10 mA: the 1 dB compression point is about 19 mA at 10 GHz, and 12 mA at 3 GHz at 300 K. At 6.6 K, the output remains linear over its vertical range, although it is important to reiterate the limited photocurrent tested ($\lesssim$ 10 mA) due to the reduced responsivity at this temperature.

The linearity of the MUTC-PD is a measure of its charge carriers' ability to respond to RF frequencies while traveling through the device. As more carriers are generated with increased optical excitation, their transit time can be influenced by a combination of thermal and space-charge effects. In the former, a hotter junction would slow charge transport as a result of reduced carrier mobility due to phonon scattering, especially under zero-bias conditions. In the case of space-charge effects, the large amount of photogenerated carriers oppose the built-in electric field, resulting in slower charge transport. The higher electric current would also lead to increased voltage drops throughout the device, which would further reduce the electric field available for drift.

As such, the onset of saturation at lower photocurrents at 0 V is unsurprising due to the increased sensitivity to the space-charge screening effect [6], which is typically counteracted through large (negative) biases: the stronger the potential, the higher the compression point for MUTC-PDs like our device [19,21,25]. However, it is noteworthy that this compression appears to initiate at lower currents at 300 K (orange data points) than it does at 80 K (magenta data points) for both 3 GHz and 10 GHz, to the extent that the maximum RF power observed at 10 GHz in these tests is 8 dB higher at 80 K than 300 K [Fig. 4(d)]. We believe this is due to thermal effects. Under zero-bias conditions, charge carriers in the MUTC-PD have likely not reached their saturation velocities. This means that transit across the depleted absorber region would depend on carrier mobility [30]. Due to a much higher electron mobility in InGaAs—the absorber material—at 80 K than 300 K, with a peak near 60 K [31], a faster electron transit is expected at 80 K than 300 K; i.e., the onset of compression should occur at higher currents, as observed in Figs. 5(c) and 5(d). Although such interesting features require further investigation, our present results confirm the ability of MUTC-PDs to attain highly linear OE conversion for $\gtrsim$10 mA photocurrents at cryogenic temperatures, with maximum output powers—under C-band exposure—limited primarily by the temperature-dependent bandgap and not other deleterious thermal phenomena.

4. Conclusion

In summary, we have presented a study of a high-speed MUTC-PD used as an OE transducer in cryogenic microwave photonic links. Key performance metrics such as dark current, wavelength-dependent responsivity, and RF bandwidth were explored at multiple temperatures and bias combinations. We assessed the saturation power of the device under a variety of operating

OPTICS CONTINUUM

conditions: −5 V or 0 V applied bias, 3 GHz or 10 GHz frequency, and 300 K, 80 K, or ∼4 K temperature. The results underscore the feasibility of such highly linear MUTC-PDs for optical delivery of RF signals to quantum systems in cryogenic environments and simultaneously shed light on the physical effects influencing the performance of these devices under extreme conditions. An obvious technical improvement moving forward will be to consider shorter (sub-1500 nm) wavelengths that are expected to retain cryogenic responsivities comparable to their room temperature counterparts, enabling higher RF powers and reduced heating from unconverted photons to reach the ultimate limits of linear MUTC-PD performance for RF photonic links. From a device-engineering perspective, it would be exciting to cryogenically test photodetectors specifically designed for zero-bias operation (for which an excellent summary can be found in [27]), as well as develop methods to explain some of the saturation behaviors observed here—perhaps similar to high-temperature thermal characterization approaches and models for MUTC-PDs [32,33], but focused on cryogenic environments. Such advances would continue to push forward both the experimental practicality and theoretical understanding of cryogenic microwave photonics for quantum control, networking, and computing.

Funding. U. S. Department of Energy, Office of Science, Basic Energy Sciences, Materials Sciences and Engineering Division (ERKCK51); U.S. Department of Energy, Office of Science, Advanced Scientific Computing Research (ERKJ353).

Acknowledgment. We thank A. Beling for discussions. This research was performed in part at Oak Ridge National Laboratory, managed by UT-Battelle, LLC, for the U.S. Department of Energy under contract no. DE-AC05-00OR22725. The Quantum Collaborative, led by Arizona State University, provided valuable expertise and resources for this research.

Disclosures. The authors declare no conflicts of interest.

Data Availability. Data available from the authors on request.

References

1. S. Pirandola and S. L. Braunstein, "Unite to build a quantum internet," Nature **532**(7598), 169–171 (2016).
2. P. Krantz, M. Kjaergaard, and F. Yan, *et al.*, "A quantum engineer's guide to superconducting qubits," Appl. Phys. Rev. **6**(2), 021318 (2019).
3. A. Morello, J. J. Pla, and P. Bertet, *et al.*, "Donor spins in silicon for quantum technologies," Adv. Quantum Technol. **3**(11), 2000005 (2020).
4. S. Krinner, S. Storz, and P. Kurpiers, *et al.*, "Engineering cryogenic setups for 100-qubit scale superconducting circuit systems," EPJ Quantum Technol. **6**(1), 2 (2019).
5. J. Yao, "Microwave photonics," J. Lightwave Technol. **27**(3), 314–335 (2009).
6. V. J. Urick Jr., J. D. McKinney, and K. J. Williams, *Fundamentals of Microwave Photonics* (Wiley, 2015).
7. F. Lecocq, F. Quinlan, and K. Cicak, *et al.*, "Control and readout of a superconducting qubit using a photonic link," Nature **591**(7851), 575–579 (2021).
8. F. Thiele, T. Hummel, and M. Protte, *et al.*, "Opto-electronic bias of a superconducting nanowire single photon detector using a cryogenic photodiode," APL Photonics **7**(8), 081303 (2022).
9. J. A. Brevik, D. Lee, and A. E. Fox, *et al.*, "Bipolar waveform synthesis with an optically driven Josephson arbitrary waveform synthesizer," IEEE Trans. Appl. Supercond. **32**(9), 1–8 (2022).
10. J. Nissilä, T. Fordell, and K. Kohopää, *et al.*, "Driving a low critical current Josephson junction array with a mode-locked laser," Appl. Phys. Lett. **119**(3), 032601 (2021).
11. Y. M. Zhang, V. Borzenets, and N. Dubash, *et al.*, "Cryogenic performance of a high-speed GaInAs/InP p-i-n photodiode," J. Lightwave Technol. **15**(3), 529–533 (1997).
12. K. Yoshino, Y. Muramoto, and T. Furuta, *et al.*, "High-speed uni-travelling-carrier photodiode module for ultra-low temperature operation," Electron. Lett. **41**(18), 1030–1031 (2005).
13. H. Ito, T. Furuta, and S. Kodama, *et al.*, "10 Gbit/s operation of uni-travelling-carrier photodiode module at 2.6 K," Electron. Lett. **44**(2), 149–150 (2008).
14. Y. Hashimoto, H. Suzuki, and M. Maruyama, *et al.*, "40 Gbit/s operation of superconductive single flux quantum digital integrated circuit with optical data input," Electron. Lett. **45**(1), 87–88 (2009).
15. H. Suzuki, "Evaluation of uni-traveling carrier photodiode performance at low temperatures and applications to superconducting electronics," in *Photodiodes*, J.-W. Shi, ed. (IntechOpen, 2011), chap. 2.
16. J. Davila-Rodriguez, H. Leopardi, and T. M. Fortier, *et al.*, "Temperature dependence of nonlinearity in high-speed," *high-power photodetectors, IEEE Photonics Conference* p. 8116021 (2017).
17. J. Davila-Rodriguez, J. D. Teufel, and J. A. Aumentado, *et al.*, "High-speed photodetection and microwave generation in a sub-100 mK environment," *CLEO* p. SF2N.1 (2019).

OPTICS CONTINUUM

18. K. Multani, W. Jiang, and E. A. Nanni, *et al.*, "Characterization of millimeter-wave superconducting circuits with an optically-driven cryogenic source," *CLEO* p. FM2E.2 (2023).
19. A. Beling, X. Xie, and J. C. Campbell, "High-power, high-linearity photodiodes," Optica **3**(3), 328–338 (2016).
20. D.-H. Jun, J.-H. Jang, and I. Adesida, *et al.*, "Improved efficiency-bandwidth product of modified uni-traveling carrier photodiode structures using an undoped photo-absorption layer," Jpn. J. Appl. Phys. **45**(4B), 3475–3478 (2006).
21. Z. Li, H. Pan, and H. Chen, *et al.*, "High-saturation-current modified uni-traveling-carrier photodiode with cliff layer," IEEE J. Quantum Electron. **46**(5), 626–632 (2010).
22. E. Rouvalis, F. N. Baynes, and X. Xie, *et al.*, "High-power and high-linearity photodetector modules for microwave photonic applications," J. Lightwave Technol. **32**(20), 3810–3816 (2014).
23. M. Woodson, S. Estrella, and E. Fodor, *et al.*, "An overview of high-power photodiodes for RF applications," Proc. SPIE **11685**, 116850I (2021).
24. Y. Tian, B. Xiong, and C. Sun, *et al.*, "Ultrafast MUTC photodiodes over 200 GHz with high saturation power," Opt. Express **31**(15), 23790–23800 (2023).
25. S. Estrella, L. A. Johansson, and M. L. Mashanovitch, *et al.*, "High-power MUTC photodetectors for RF photonic links," Proc. SPIE **9747**, 97471X (2016).
26. J. S. Morgan, K. Sun, and Q. Li, *et al.*, "High-power flip-chip bonded modified uni-traveling carrier photodiodes with −2.6 dBm RF output power at 160 GHz," *IEEE Photonics Conference* p. 8527260 (2018).
27. F. Yu, K. Sun, and Q. Yu, *et al.*, "High-speed evanescently-coupled waveguide type-II MUTC photodiodes for zero-bias operation," J. Lightwave Technol. **38**(24), 6827–6832 (2020).
28. E. Abe and K. Sasaki, "Tutorial: Magnetic resonance with nitrogen-vacancy centers in diamond—microwave engineering, materials science, and magnetometry," J. Appl. Phys. **123**(16), 161101 (2018).
29. S. Vaidya, X. Gao, and S. Dikshit, *et al.*, "Quantum sensing and imaging with spin defects in hexagonal boron nitride," Adv. Phys.: X **8**(1), 2206049 (2023).
30. W. Xiong, Z. Peng, and R. Yao, *et al.*, "Systematic analysis of a modified uni-traveling-carrier photodiode under high-power operating conditions," Photonics **10**(4), 471 (2023).
31. J. Oliver, L. F. Eastman, and P. D. Kirchner, *et al.*, "Electrical characterization and alloy scattering measurements of LPE $Ga_xIn_{1-x}As$/InP for high frequency device applications," J. Cryst. Growth **54**(1), 64–68 (1981).
32. H. Chen, A. Beling, and H. Pan, *et al.*, "A method to estimate the junction temperature of photodetectors operating at high photocurrent," IEEE J. Quantum Electron. **45**(12), 1537–1541 (2009).
33. Y. Shen, J. Gaskins, and X. Xie, *et al.*, "Thermal analysis of high-power flip-chip-bonded photodiodes," J. Lightwave Technol. **35**(19), 4242–4246 (2017).